

Spatial and temporal plasticity of synaptic organization in anterior cingulate cortex following peripheral inflammatory pain: multi-electrode array recordings in rats

Yun-Fei Lu^{1,2,*}, Yan Wang^{1,2,*}, Ying He^{3,*}, Fu-Kang Zhang³, Ting He^{1,2}, Rui-Rui Wang^{1,2,3}, Xue-Feng Chen^{1,2}, Fei Yang^{1,2}, Ke-Rui Gong³, Jun Chen^{1,2,3}

¹*Institute for Biomedical Sciences of Pain and Institute for Functional Brain Disorders, Tangdu Hospital, The Fourth Military Medical University, Xi'an 710038, China*

²*Key Laboratory of Brain Stress and Behavior, PLA, Xi'an 710038, China*

³*Institute for Biomedical Sciences of Pain, Capital Medical University, Beijing 100069, China*

*These authors contributed equally to this work.

Corresponding author: Jun Chen. E-mail: junchen@fmmu.edu.cn

© Shanghai Institutes for Biological Sciences, CAS and Springer-Verlag Berlin Heidelberg 2014

ABSTRACT

To explore whether experiencing inflammatory pain has an impact upon intracortical synaptic organization, the planar multi-electrode array (MEA) technique and 2-dimensional current source density (2D-CSD) imaging were used in slice preparations of the anterior cingulate cortex (ACC) from rats. Synaptic activity across different layers of the ACC was evoked by deep layer stimulation through one electrode. The layer-localization of both local field potentials (LFPs) and the spread of current sink calculated by 2D-CSD analysis was characterized pharmacologically. Moreover, the induction of long-term potentiation (LTP) and changes in LTP magnitude were also evaluated. We found that under naïve conditions, the current sink was initially generated in layer VI, then spread to layer V and finally confined to layers II–III. This spatial pattern of current sink movement typically reflected changes in depolarized sites from deep layers (V–VI) to superficial layers (II–III) where intra- and extra-cortical inputs terminate. In the ACC slices from rats in an inflamed state (for 2 h) caused by intraplantar bee-venom injection, the spatial profile of intra-ACC synaptic organization was significantly changed,

showing an enlarged current sink distribution and a leftward shift of the stimulus-response curves relative to the naïve and saline controls. The change was more distinct in the superficial layers (II–III) than in the deep site. In terms of temporal properties, the rate of LTP induction was significantly increased in layers II–III by inflammatory pain. However, the magnitude of LTP was not significantly enhanced by this treatment. Taken together, these results show that inflammatory pain results in distinct spatial and temporal plasticity of synaptic organization in the ACC, which may lead to altered synaptic transmission and modulation.

Keywords: anterior cingulate cortex; multi-electrode array; synaptic plasticity; intracortical synaptic organization; pain

INTRODUCTION

Chronic pain is often accompanied by various comorbidities in the brain, such as anxiety, insomnia, amnesia, cognitive impairment, disability and depression^[1], but the underlying mechanisms are largely unknown. It is widely known that pain perception is generated in the brain, which in turn

has an endogenous modulatory system to stop pain under certain conditions^[2–4]. However, it has gradually been appreciated that the endogenous analgesic system does not work well under pathological conditions^[5]. Many human brain imaging data support the hypothesis that chronic pain results in structural and functional plasticity, leading to brain dysfunctions and comorbidities^[6,7]. To reveal what occurs in the brain after persistent pain, the functions of neuronal circuits (synaptic organization) should be examined at the cortical level in animal models. Imaging data show similar activation of brain regions by experimental persistent pain using the rodent formalin test^[8–10], suggesting the feasibility of studying the impact of pain on cortical functions in animals.

The anterior cingulate cortex (ACC) is involved in the affective or emotional aspects of pain in both humans and animals^[11–21]. Neuroimaging data show that more and longer unpleasant, noxious stimuli result in a more intense and extensive 'lighting-up' of the ACC in humans^[6,7,22] and the same noxious stimuli also activate this area in animals^[8–10], implicating the existence of spatiotemporal changes or the re-organization of synaptic connections (the 'network') in this region. In behavioral studies, bilateral lesions of the ACC or injection of lidocaine into the anterior cingulum bundle alleviate inflammatory hypersensitivity in animals^[23–27], whereas electrical stimulation of the ACC facilitates the tail-flick reflex^[28], suggesting involvement of the ACC in the facilitation of pain-related behaviors. Electrophysiological studies have identified pain-related neurons in the animal ACC (most are pyramidal cells) with their somata mainly confined to layers V–VI^[29–36]. Pain-related neurons have also been identified in the human ACC^[37]. The above evidence strongly supports the idea that the ACC is an important cortical region that receives and processes nociceptive information from the periphery.

More recently, using whole-cell patch-clamp recording, our group revealed enhanced excitatory synaptic transmission and decreased inhibitory synaptic transmission in acutely-dissociated ACC slices from rats pre-conditioned with 2 h of peripheral inflammatory pain induced by subcutaneous (s.c.) injection of bee venom (BV)^[38]. Therefore, BV-associated disruption of the balance between excitatory and inhibitory inputs to the ACC pyramidal cells may lead to instability of the intracortical

synaptic organization and probably alters pain-related behaviors^[12,26,39]. This is of particular importance and needs to be tested at the network level to determine whether the stability of intracortical synaptic organization can be changed by a pre-existing inflammatory pain state.

The neuronal network in the ACC is formed by synaptic organization across layers I, II–III, and V–VI that involves both pyramidal cells and excitatory or inhibitory local interneurons^[18,33,36,40]. The pain-related neurons in the ACC of rats are categorized into two functional types^[36]: (1) nociception-specific neurons with cell bodies mainly in layers III and V–VI, apical dendrites extending to layer I, and axons projecting to subcortical structures; and (2) noxious-tap (neurons responding to noxious mechanical and tap stimuli) pyramidal cells with somata mainly in layers V–VI, apical dendrites extending to layer I, and recurrent collateral axons projecting widely from layers V–VI to layers II–III. This suggests that a population of pain-related pyramidal neurons such as the noxious-tap type may play important roles in the neuronal circuitry in the ACC. Another study identified two populations of pain-related pyramidal neurons in the rabbit ACC (layers II–IIIab, and Vab) that show distinct durations of excitatory post-synaptic potentials (EPSPs)^[33]. The short-duration EPSP (≤ 200 ms) was suggested to reflect thalamic-mediated nociceptive responses, while the long-duration EPSP (≥ 350 ms) was believed to be mediated by intracortical integration through collateral axonal discharges. The circuits in the ACC can also be activated by noxious stimulation *in vivo*^[41]. Collectively, these results emphasize the importance of the intracortical neuronal network in responding to nociceptive input and in maintaining the functional stability of the ACC.

The intra-ACC plasticity, such as short-term plasticity (STP), LTP, and long-term depression (LTD) evoked by electrical stimulation in layers V–VI, is a good synaptic model that has recently been established in a coronal brain slice preparation using planar multi-electrode array (MEA) recordings^[42–44]. Moreover, dynamic time-variant changes in 2-dimensional current source density (2D-CSD) imaging have been successfully applied to planar 8×8 MEAs (64 channels) by which the time-variant movement of current sink and source images can be traced in a specific anatomical structure in the brain. This makes it feasible to study the synaptic plasticity of brain networks both in

time and space^[45-50]. In the current study, we combined the planar MEA technique with 2D-CSD imaging in rat coronal ACC slices to study the plasticity of intra-ACC synaptic organization both spatially and temporally under BV-preconditioning and saline control conditions.

MATERIALS AND METHODS

Drug Preparation

The BV solution was lyophilized whole venom from *Apis mellifera* (Sigma, St. Louis, MO) dissolved in sterile saline. AP5 (*D,L*-2 amino-5-phosphonopentanoic acid; Sigma) and bupivacaine were dissolved in deionized water as stock solutions and frozen in aliquots. They were diluted to the target concentration in artificial cerebrospinal fluid (ACSF) immediately before use. CNQX (6-cyano-7-nitroquinoxaline-2, 3-dione; Sigma-Aldrich) was dissolved in dimethylsulfoxide (final concentration 0.1%).

Animals

Male albino Sprague-Dawley rats (3–4 weeks old, weighing 80–120 g) were obtained from the Laboratory Animal Center of the Fourth Military Medical University (FMMU) and Capital Medical University (CCMU). The animals were housed individually with food pellets and tap water *ad libitum* under standard laboratory conditions (12 h light/dark cycle, 22–26°C, humidity 40–60%). The experimental protocols were approved by the Institutional Animal Care and Use Committees of FMMU (Permit number: SCXK2007-007) and CCMU (Permit number: SCXK2007-004), and carried out in accordance with the National Institutes of Health Guide for the Care and Use of Laboratory Animals (NIH Publications No. 80-23 revised 1996), the UK Animals (Science Procedures) Act 1986 and associated guidelines, and the European Communities Council Directive of 24 November 1986 (86/609/EEC). All animals were also maintained and cared for in accordance with the guidelines set forth by the International Association for the Study of Pain^[51], with efforts made to minimize the number of animals and prevent suffering.

Rats were randomly divided into four groups: (1) without any treatment as the naïve group; (2) with s.c. injection of 0.9% sterile saline as the physiological pain control (transient pain state); (3) with s.c. injection of BV as the inflammatory pain model (persistent pain state)^[38,52-54],

and (4) with s.c. pre-injection of 0.6 mL bupivacaine (0.25%) into the BV injection site (10 min in advance) to block nociceptive activity^[55-58].

Induction of Persistent Pain

A volume of 50 μ L saline containing 0.2 mg bee venom was used throughout, as this is the optimal dose to induce long-lasting pain-related behavioral responses^[38,52,59]. The BV solution was injected s.c. into the posterior plantar surface of one hind-paw. The same volume of saline was injected into the same site as a control.

Preparation of Acute ACC Slices

The preparation of brain slices containing ACC was as previously described^[39,42]. Rats were deeply anaesthetized with sodium pentobarbital (40 mg/kg, i.p.) 2 h after BV or saline injection and then sacrificed by decapitation. We chose 2 h as the time point because: (1) the temporal summation of 2 h of spike discharges from a peripheral injury site to the spinal dorsal horn and higher brain structures has been demonstrated to be sufficient for the induction of full central plasticity (sensitization)^[38,48,54,59,60], and (2) behaviorally, the transition from a decline of spontaneous paw flinching responses to the peak timing of both thermal and mechanical hyperalgesia serves as a biomarker of the neuronal state studied in our previous and present work^[38]. After decapitation, the whole brain was removed rapidly and submerged in ice-cold oxygenated ACSF containing (in mmol/L): NaCl 124, KCl 3.3, KH_2PO_4 1.2, MgSO_4 2.4, CaCl_2 2.5, NaHCO_3 26 and glucose 10, pH 7.4. After cooling for 1–2 min, the brain was trimmed appropriately and glued to the ice-cold stage of vibrating tissue slicer (DTK1000, Dosaka-EM Co. Ltd., Japan), then submerged in ice-cold, oxygenated ACSF. Note that only the ACC contralateral to the BV or saline injection site was used in this investigation. Coronal slices at an angle of 15° to the vertical line containing the ACC (bregma: 2.28–1.56 mm) were cut at 350 μm ^[61] (Fig. 1) and gently transferred to a chamber containing ACSF gassed with 95% O_2 and 5% CO_2 and incubated at room temperature for 2 h before electrophysiological recording.

Preparation of MEA

A 64-channel multi-electrode dish system (MED-64, Alpha-

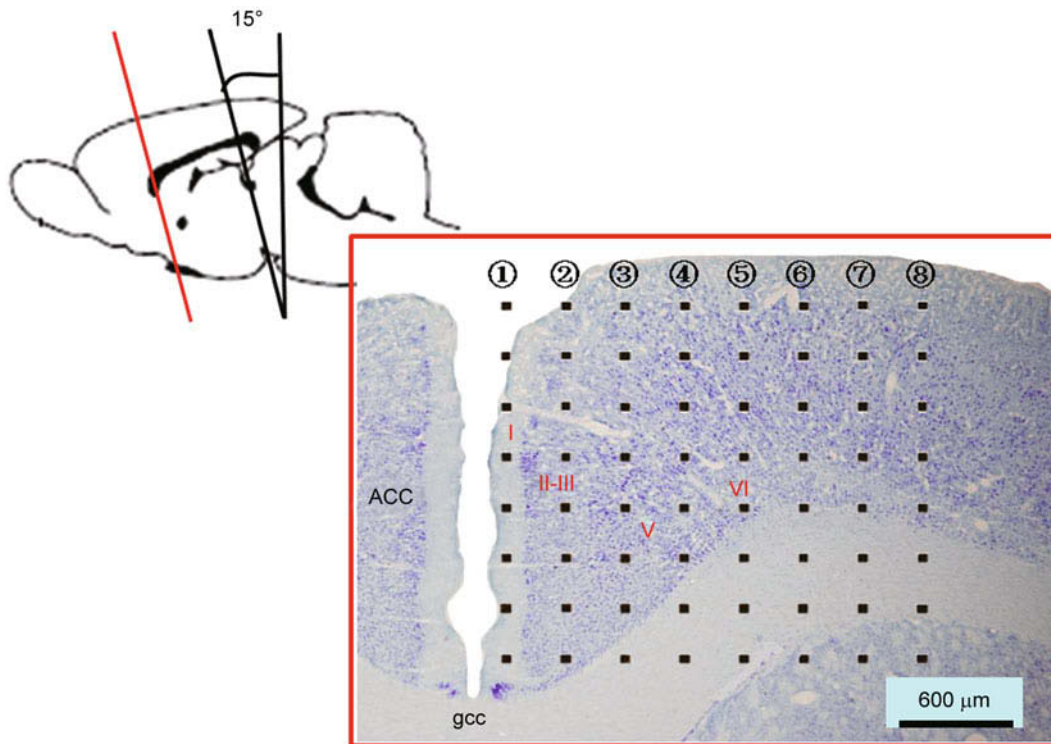


Fig. 1. Cutting angle of the ACC slices. Coronal slices containing the ACC were cut at 15° to the vertical. A microphotograph showing the relative position of the laminae of the ACC and the 8 × 8 array of the MED-64 probe (aligned from left to right in numerical order: row 1, 1–8, as shown in the figure; row 2, 9–16; row 3, 17–24; row 4, 25–32; row 5, 33–40; row 6, 41–48; row 7, 49–56; and row 8, 57–64). ACC, anterior cingulate cortex; gcc, genu of the corpus callosum. 1% cresyl violet staining. Inter-electrode distance, 300 μm; scale bar, 600 μm.

Med Scientific, Japan) was used for local field potential (LFP) recording. The procedures for preparing the MEA were as previously described^[45–50]. The size of each electrode was 50 × 50 μm², and all 64 were arranged in an 8 × 8 square with an inter-electrode distance of 300 μm to cover an area of 4.4 mm². Before use, the surface of a new MED-64 probe was treated with 0.1% polyethyleneimine (Sigma; P-3143) in 25 mmol/L borate buffer (pH 8.4) overnight at room temperature. Besides, the surface of the MED-64 probe was rinsed with sterile distilled water immediately before use. At the end of each recording session, the probe was cleaned carefully with deionized water to maintain stable electrode properties. In general, each MED-64 probe was re-used for 30–40 recording sessions, each with a mean duration of 4–6 h.

Electrophysiological Recordings

After 2-h incubation, under an inverted microscope (IX71,

Olympus, Japan), a slice was gently placed on the MED-64 probe, with the ACC area covering the whole 8 × 8 array. Once the ACC had settled on the probe, a nylon-mesh anchor (SHD-22L, Harvard, USA) was placed over the slice to ensure immobilization during the recording session. The position of the MEA relative to the cytoarchitecture of the ACC across layers I (1st vertical row), II–III (2nd vertical row), V (3rd vertical row) and VI (4th–5th vertical rows) stained by the Nissl method was clearly visible (Fig. 1). The slice was continuously perfused with ACSF oxygenated with 95% O₂ and 5% CO₂ at 2 mL/min with the assistance of a peristaltic pump (Peri-Star, WPI, USA) at room temperature. After 20-min incubation, the optimal stimulation site was determined by selecting channels covering ACC layers V–VI and finally the electrode that evoked maximal network responses at a moderate intensity was chosen as the stimulation site while the remaining 63 electrodes were used for recording. For test stimulation,

a bipolar, biphasic constant current pulse (2×0.1 ms) at intensities ranging from 10 μ A to 199 μ A was generated from the MED Conductor and applied to the stimulus site. Evoked LFPs were amplified by a 64-channel amplifier and digitized at 20 kHz. The digitized data were displayed on the monitor screen and stored on the hard disk of a microcomputer.

Experimental Protocols

After determining the optimal simulation site and allowing the responses to stabilize for ~ 30 min, input-output (I-O) curves were first established for each group by measuring the LFP amplitude in response to a series of suprathreshold stimuli. Intensities >199 μ A were not used to avoid damage to the microelectrode^[48,49]. Stable baseline recordings were monitored for at least 30 min before the induction of LTP. LTP was induced by long train of theta-burst stimulation (TBS) which has a high induction rate as suggested by our previous reports^[42]. Briefly, the TBS protocol consisted of 10 trains of bursts of 4 pulses at 100 Hz at 200-ms intervals^[42]. To standardize the tetanization strength in different experiments, the TBS strength was set at the intensity around half of the maximum amplitude of LFPs based on the I-O values. After TBS conditioning, a test stimulus was delivered once every 10 min for >2 h to detect any changes in the magnitude and duration of LFPs. In some experiments, a pharmacological approach was used to determine whether the LFPs were mediated by pre-synaptic neurotransmitter release driven by action potentials or by post-synaptic ionic glutamate receptors^[31,44,62]. To identify presynaptic mediation, the slices were perfused for 10 min with tetrodotoxin (TTX, 0.5 and 1.0 μ mol/L) or high Mg^{2+} -low Ca^{2+} (hMg-ICa) solution (the concentration of $CaCl_2$ was lowered to 0.25 mmol/L while the concentration of $MgSO_4$ was raised to 4.0 mmol/L in the ACSF). To identify post-synaptic mediation, the slices were perfused for 10 min with the glutamate non-NMDA receptor antagonist CNQX (10 μ mol/L) or the glutamate NMDA receptor antagonist AP5 (100 μ mol/L). The drugs were perfused at 2 mL/min, and replaced by fresh ACSF 10 min after application. The recordings were continued until normal synaptic responses returned.

Two-Dimensional Current-Source Density Analysis

To characterize the spatial distribution of current sinks and

sources in layers (I, II–III, V, and VI) in any direction in the plane of the ACC slice^[48], the current-source density over the 2D-CSD was computed. In general, the 2D current density I_m in the presence of a field potential Φ is given as

$$I_m = - \left[\sigma_x \frac{\partial^2 \Phi}{\partial x^2} + \sigma_y \frac{\partial^2 \Phi}{\partial y^2} \right].$$

Since the measured field potential (Φ_{ij}) was recorded on a planar array of 64 electrodes, the second partial derivatives at the centers of particular electrodes could be computed from the LFP measured at that electrode and its neighbors as

$$\frac{\partial^2 \Phi_{i,j}}{\partial x^2} \approx \frac{(\Phi_{i+1,j} - 2\Phi_{i,j} + \Phi_{i-1,j})}{\Delta x^2}, \quad \frac{\partial^2 \Phi_{i,j}}{\partial y^2} \approx \frac{(\Phi_{i,j+1} - 2\Phi_{i,j} + \Phi_{i,j-1})}{\Delta y^2}.$$

By considering the medium as ohmic with homogeneous conductance ($\sigma_x = \sigma_y = \sigma$), and under the assumption of equidistant electrodes ($\Delta x = \Delta y = \Delta$), the normalized CSD ($I'_{i,j}$) was defined and computed as

$$I'_{i,j} \equiv \frac{\Delta^2 I_{i,j}}{\sigma} \approx 4\Phi_{i,j} - (\Phi_{i+1,j} + \Phi_{i-1,j} + \Phi_{i,j+1} + \Phi_{i,j-1}).$$

With the normalized CSD values at the centers of the electrodes, it became possible to compute the density at any point (x, y) within the 8×8 array using bilinear interpolation. After all the above calculations, we used the color yellow to represent positive currents (sources), blue to represent negative currents (sinks), and black to map zero current. Finally, CSD images at selected time points were plotted across all 64 recording sites for each group of slices.

Data Analysis and Statistics

To analyze the components of LFPs, the peak latency of each LFP in layers I, II–III and V–VI was measured. The onset latency of each component was not included in the current study due to the variety of the waveforms under different conditions. To quantify the I-O relationship, the amplitudes of LFPs were analyzed offline by MED-64 Conductor. For LTP data, the amplitudes of the LFPs were normalized and expressed as a percentage of the average value measured during the last 10 min of the baseline period. Drug effects were evaluated as the difference between before and 10 min after drug infusion (when the drug effect peaked). The total number of effective LFPs ($>20\%$ baseline) reliably recorded over the ACC was counted by an experimenter unaware of the design and averaged across slices for each group. Data sets include

results from only one slice per rat (n = number of slices). All data are expressed as mean \pm SEM. When necessary, Student's t test (paired and two-independent sample) or one-way ANOVA (*post-hoc* Fisher's PLSD) was used to determine statistical significance. $P < 0.05$ was considered statistically significant.

RESULTS

Spatial Distribution of Intra-ACC Responses Evoked by Deep-Layer Stimulation

Based on previous reports using the planar MEA technique on coronal ACC slices^[31,42,43], we first re-examined the spatial distribution of intra-ACC responses evoked from the deep layers in slices from naïve rats. Electrical stimulation through an electrode (Fig. 2A) in layer VI resulted in widespread LFP responses across layer V, to layers II–III and I. Both the amplitude and the spatial size of the network LFP responses were intensity-dependent (Fig. 2A). To further understand the components of LFPs in layers I, II–III, and V–VI, typical waveforms from each layer were analyzed (Fig. 2B). The LFPs ($n = 9$ in all cases) in layer I were consistently composed of a prolonged positive-going component (P1, peak latency 6.53 ± 0.44 ms) sometimes followed by a late negative-going (N1) component. The LFPs in layers II–III and V were composed of an early transient P1 (1.61 ± 0.10 ms) followed consecutively by a short N1 (3.36 ± 0.19 ms), a long N2 (7.53 ± 0.43 ms) and a longer late P2 (13.3 ± 0.73 ms). The LFPs in layers V–VI were different from the other layers; they were composed of a short P1 (2.62 ± 0.16 ms), a longer N1 (4.88 ± 0.31 ms), and a late small P2 (11.03 ± 0.76 ms).

Pharmacological Identification of Each Component of Intra-ACC LFP Responses

To identify each component of the LFPs, TTX and hMg-ICa solution were applied to ACC slices from naïve rats. Perfusion with $0.5 \mu\text{mol/L}$ TTX did not completely block the LFPs in the whole ACC although the inhibitory rate was layer-related (74% for layer I, 41% for layers II–III, and 16% for layers V–VI), while $1.0 \mu\text{mol/L}$ TTX completely abolished the LFPs in layers I and V–VI (Fig. 3A). However, in layers II–III, the P1, N2 and P2 components were completely abolished but the N1 component remained incompletely inhibited. Therefore, the N1 component of layers II–III was

not included in the quantitative analysis due to its TTX-resistant property (Fig. 3B). Substitution of the ACSF with hMg-ICa bath solution resulted in robust abolition of the late N1 component in layer I, N2 and P2 in layers II–III, and N1 and P2 in layers V–VI, while the early part of P1 in layer I, P1 and N1 in layers II–III, and P1 in layers V–VI were incompletely inhibited (Fig. 3). Furthermore, bath perfusion with CNQX ($10 \mu\text{mol/L}$) gave the same results as hMg-ICa solution (Fig. 4). However, the same treatment with AP5 ($100 \mu\text{mol/L}$) did not have any effect (Fig. 4). Taken together, these results suggested that hMg-ICa- and CNQX-sensitive components are likely to represent field excitatory postsynaptic potentials (fEPSPs), whereas hMg-ICa- and CNQX-resistant but TTX-sensitive components are likely to be presynaptic volleys. The part of the N1 component in layers II–III remaining after either hMg-ICa or CNQX treatment may be associated with recurrent collateral axonal responses from layer V^[33,36]. Based on these results, we next focused on the fEPSPs to determine whether their spatial and temporal properties can be changed by experimental conditioning protocols and the pre-conditioned peripheral inflammatory state.

Induction of LTP in the ACC by Deep-Layer Stimulation

In ACC slices from naïve rats (left panel, Fig. 5A), electrical stimulation was applied to layer V through a planar electrode at the intensity ($90 \mu\text{A}$, 2×0.1 ms) of half-maximal response (according to I–O curves in Fig. 7). LTP was stably induced in layers II–III and V–VI when a long-train TBS conditioning stimulus (CS) was applied (Figs 5A, 9A1/A2 and 10 for naïve rats). Similar to our previous results^[42], the LTP induction rate was 61.53% ($n = 13$) from layers II–III and V–VI. From the time-variant 2D-CSD images (Fig. 5B), the intra-ACC current sink was spatially confined to layers II–III and V–VI and centered in layer III in the pre-CS state. Temporally, the current sink started with depolarization from layer VI to layer V at 3.0–6.0 ms, spread from layers V–VI to layers II–III at 9.0 ms, and was confined to layers II–III from 11.0 ms until its gradual decline. Compared with pre-CS, the profile and intensity of the current sink increased significantly 120 min post-CS (lower panel in Fig. 5B). Comparisons of the LFPs and CSDs at each corresponding site across the 64 electrodes were made between pre-CS and 120 min post-CS (right panels in Fig. 5A). This result suggested that long-train CS

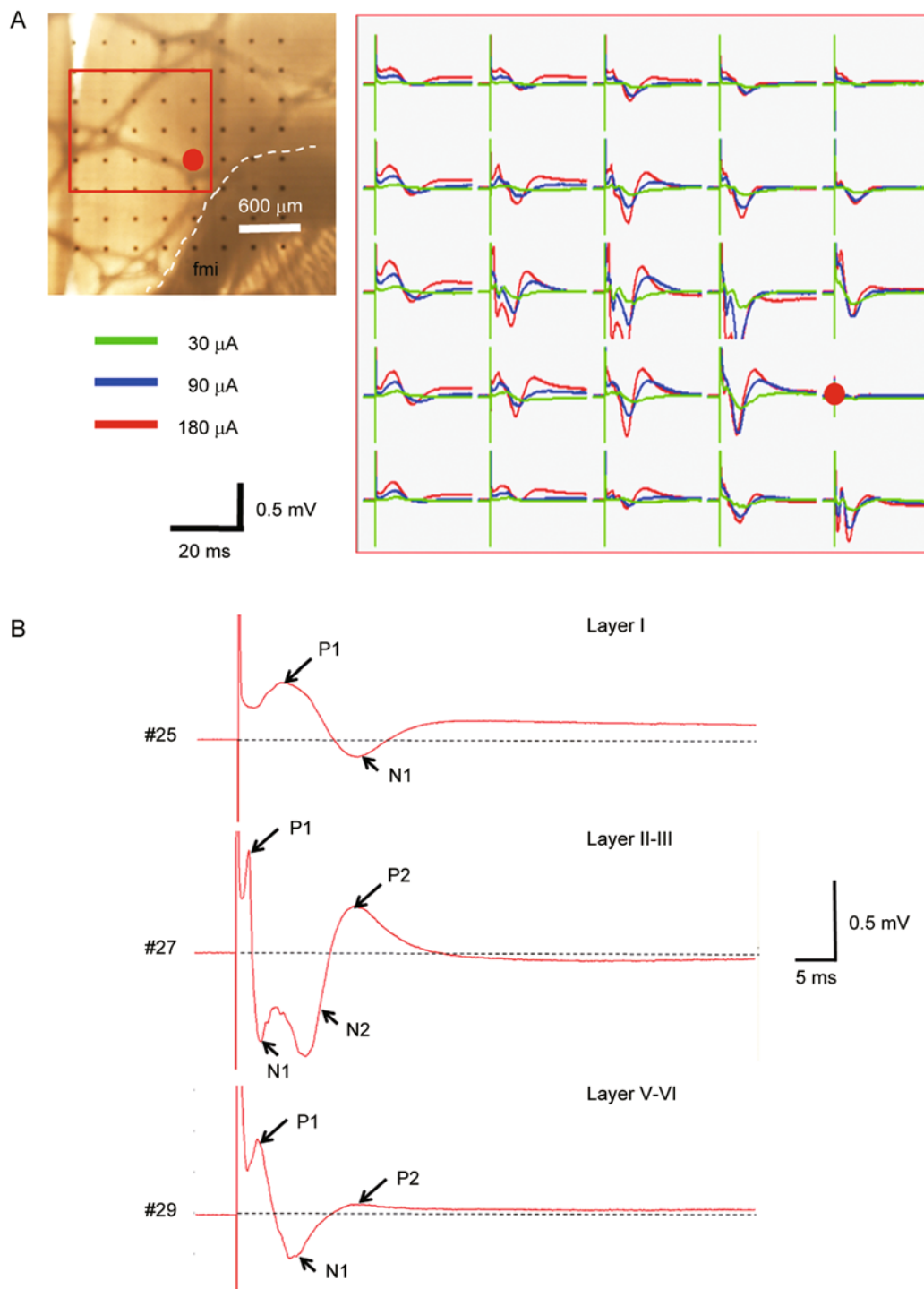


Fig. 2. Intensity-dependent LFP responses in the ACC and identification of LFP components. **A**, Left panel: location of the MEA on an ACC slice in a representative recording. Right panel: superimposed LFP network profiles recorded in response to different stimulus intensities confined to the red rectangle indicated in the left panel. Red dot indicates the stimulating electrode. Green traces indicate 30 μA , blue 90 μA , and red 180 μA . Scale bar, 600 μm . **B**: Identification of LFP components recorded in different layers of the ACC in response to a stimulating site in deep layers. Vertical scale indicates amplitude, horizontal scale indicates time. Fmi: forceps minor of the corpus callosum.

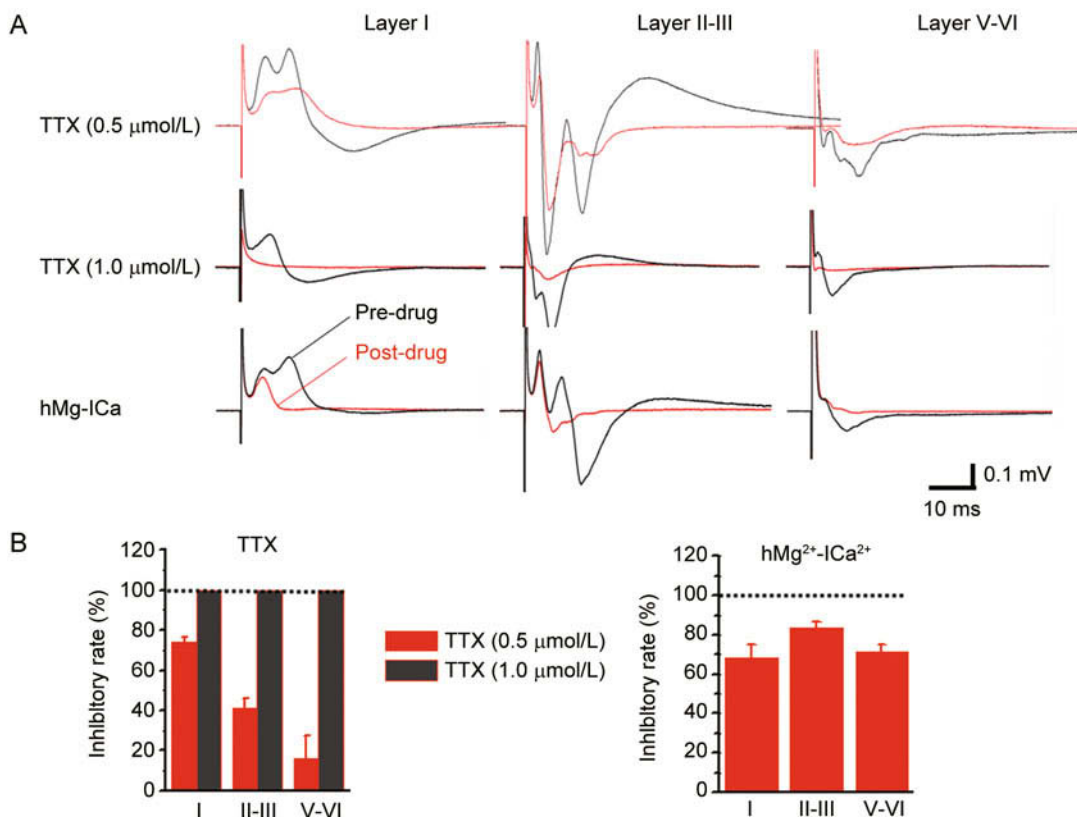


Fig. 3. Pharmacological identification of LFP responses spanning all layers in the ACC. A: Typical raw traces of LFPs before treatment (black traces), and 10 min after perfusion with TTX (upper and middle panels, red traces) or high Mg²⁺-low Ca²⁺ solution (0.25 mmol/L CaCl₂, 4.0 mmol/L MgSO₄) (lower panel, red traces). Vertical scale indicates amplitude, horizontal scale indicates time. B: Inhibitory rates of fEPSPs following bath application of TTX (0.5 or 1.0 μmol/L, *n* = 3 for each dose) and high Mg²⁺-low Ca²⁺ solution (*n* = 4). Note that 1.0 μmol/L TTX resulted in complete and wash-irreversible blockade of LFPs (100% inhibition), high-Mg²⁺ solution had a greater inhibitory rate in layers II-III (84%) than in layers I (69%) and V-VI (71%). Mean ± SEM.

produced a high induction rate of LTP in ACC slices from naïve rats.

Effects of Peripheral Inflammatory Pain State on the Stability of Intra-ACC Synaptic Organization

Spatial changes in intra-ACC responses to deep-layer stimulation

In ACC slices from naïve and saline-control rats, the synaptic organization remained stable in both the spatial and temporal domains. To quantify spatial changes in the synaptic network profile, we counted the number of effective LFPs (>20% of baseline) as values for comparison^[45,46,48,50]. Then spatial stimulus-response curves were plotted based upon this paradigm. The stimulus-response curves of the naïve and saline-control groups overlapped well, and both showed a plateau effect when

stimulus intensity was increased over 90 μA (Fig. 6C). However, pre-conditioning by 2 h of peripheral inflammation greatly changed the spatial structure of the synaptic organization. Figures 6A and 6B show two example recordings from ACC slices from saline-control and BV-inflamed rats. The spatial stimulus-response curve of the BV-inflamed group shifted leftward relative to the saline-control and naïve groups, and this was completely reversed by peripheral pre-blockade with bupivacaine (Fig. 6C). The stimulus intensity for the plateau effect also increased compared with naïve and saline-control. Moreover, the amplitudes of LFPs across layers I, II-III and V-VI were all significantly increased (Fig. 7). The standardized amplitudes of LFPs in layers I, II-III and V-VI of naïve, saline-control, BV-inflamed, and peripheral pre-blockade

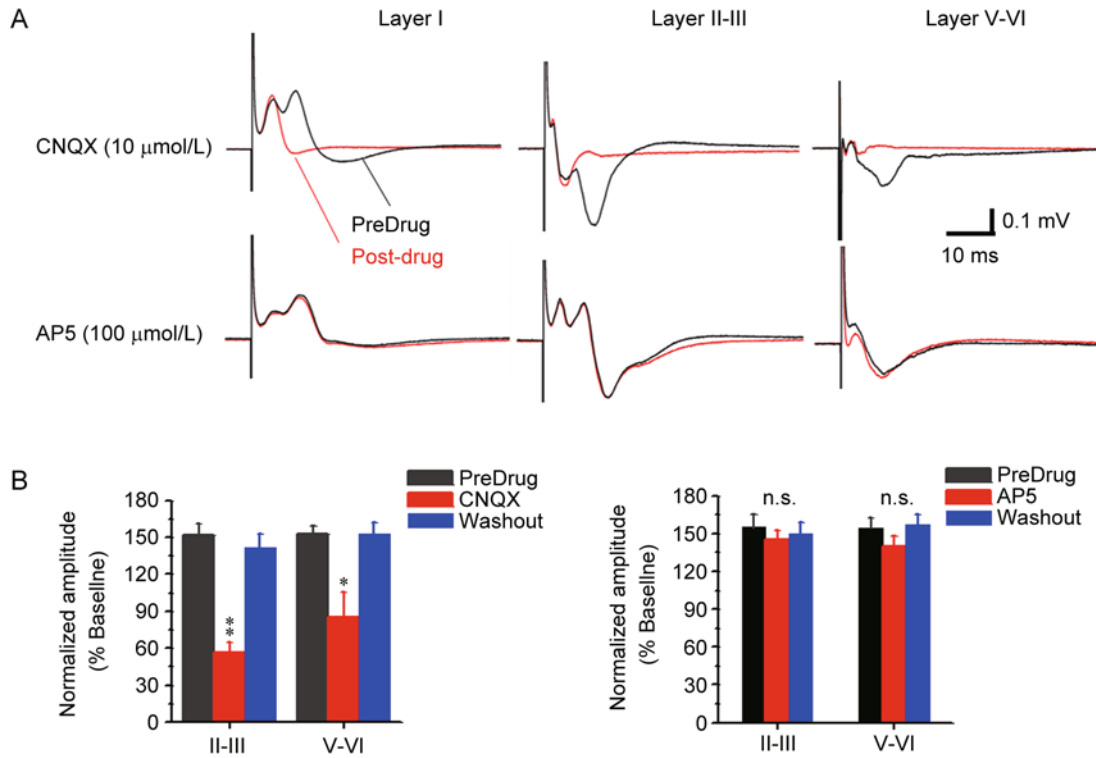


Fig. 4. Pharmacological investigation of LFP responses spanning all layers in the ACC following stimulation of deep layers. **A:** Typical raw traces of LFPs before treatment (black traces), and 10 min after perfusion with CNQX (10 $\mu\text{mol/L}$) or AP5 (100 $\mu\text{mol/L}$). Vertical scale indicates amplitude, horizontal scale indicates time. **B:** Pooled data recorded in layers II–III and V–VI. * $P < 0.05$, ** $P < 0.01$ vs pre-drug. Mean \pm SEM.

were shown in the I–O curves (lower panels in Fig. 7). Layer-specific analysis revealed the greatest enhancement of LFPs in layers II–III and less enhancement in layers V–VI in the inflammatory state (lower panels in Fig. 7). Similarly, this enhancement was also reversed by peripheral pre-blockade with bupivacaine at the BV injection site.

Temporal changes in intra-ACC responses to deep-layer stimulation Before examining the effects of the pre-conditioned peripheral inflammatory state on the induction and maintenance of LTPs, the effects of long-train TBS CS on the intra-ACC synaptic network profile were examined in naïve, saline-control and BV-inflamed rats. The synaptic connection network profile (shown as the number of fEPSPs) was not significantly changed by long-train TBS conditioning compared to the pre-conditioning results (Fig. 8A), implying that long-train CS itself did not change the intra-ACC synaptic network profile in the naïve state. The LTP induction rate (Fig. 9) was significantly higher

in layers II–III in both the saline-control and BV-inflamed groups (76.9% for both, 10/13 slices) than in the naïve group (61.5%, 8/13). However, in the deep layers V–VI, the LTP induction rate was much higher in the BV-inflamed group (69.2%, 9/13 slices) than in the saline-control and naïve groups (61.5% for both, 8/13 slices). As for the LTP recordings over 2 h, neither the peripheral inflammatory state nor transient nociception was able to further enhance the LTP amplitude in layers II–III or V–VI compared with the naïve state (Fig. 10). Nonetheless, interestingly, the induction of LTP in layers II–III occurred ~ 30 min earlier than in layers V–VI, suggesting that LTP probably occurred first at dendritic spines and dendrites (early and intermediate LTP) in layers II–III, then at the somata of the pyramidal cells in layer V (Fig. 10).

To test whether NMDA receptors are involved in rats pre-conditioned with peripheral inflammation, CNQX and AP5 were perfused through ACC slices from saline-

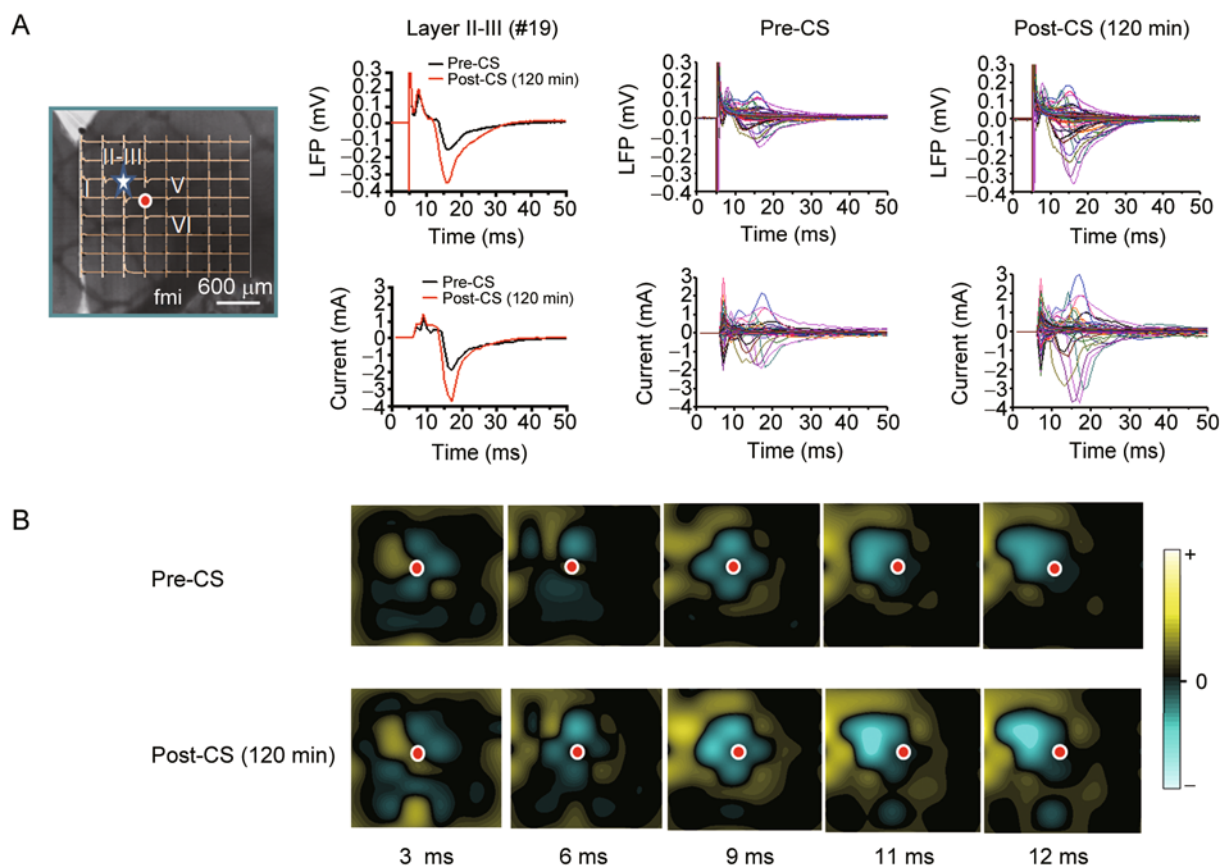


Fig. 5. 2D-CSD imaging of the time-variant spread of the spatial profile of LFP responses following TBS conditioning in the ACC of naïve rats. **A:** Left panel: location of the 8×8 MEA recording sites across layers I, II–III, and V–VI of the ACC in a slice. Right panels: effects of TBS conditioning (CS) on both LFPs (upper three) and current (lower three) responses. Red dot indicates the stimulating electrode. The asterisk indicates electrode #19 in layers II–III from which the recorded LFPs and currents (positive for source and negative for sink) were compared between pre- and post-CS (120 min). **B:** 2D-CSD images of network response profiles at five time points (3, 6, 9, 11, and 12 ms of a sweep) before and 120 min after CS. Red dots indicate the stimulating electrodes. fmi, forceps minor of the corpus callosum; Pre-CS, pre-conditioning stimulus; Post-CS, post-conditioning stimulus. Vertical color bar indicates current density for source (+, yellow) and sink (-, blue).

control and BV-inflamed rats. CNQX significantly reduced the synaptic network profile in the ACC, while AP5 did not have any inhibitory effect on the current sink in the same region (Fig. 8B), suggesting the involvement of non-NMDA receptors in the production and propagation of the intra-ACC current sink in response to deep-layer stimulation.

DISCUSSION

Spatial and Temporal Plasticity of Intracortical Synaptic Organization

The ACC is an important forebrain structure that is often

used as a cortical synaptic model for pain studies. At the individual synaptic level, temporal synaptic plasticity, including STP and LTP, has been well studied both *in vivo* and *in vitro*^[19–21,63], however, much work remains to be done at the network level to bridge the gap between activity at single synapses and behavior. Planar MEA recording from acutely dissociated and cultured brain slices is a useful technique for studying neuronal plasticity at the network level in both space and time^[49]. More recently, efforts have been made to use planar MEAs in coronal slices for intra-ACC structure or transverse slices through the medial thalamus–ACC projection pathway to study STP, LTP

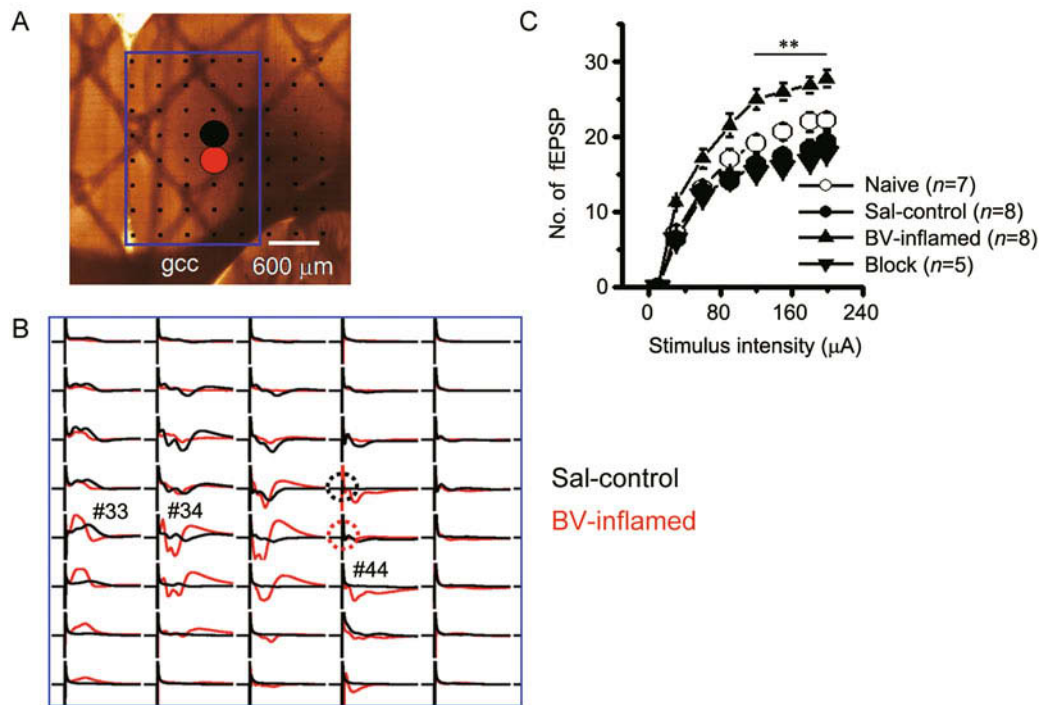


Fig. 6. MEA recordings from ACC slices from rats receiving saline or BV injection. **A:** Location of the MED-64 probe on the ACC slice during the recording session. Red and black dots indicate the electrode selected for stimulation in deep layers of the ACC after BV and saline injection, respectively. Scale bar, 600 μm ; gcc, genu of the corpus callosum. **B:** Superimposed LFP network response profiles recorded at different electrodes confined to the blue rectangle indicated in A. Dashed circles indicate the stimulating electrodes. **C:** Curves of the stimulus intensity-network response showing the mean average number of reliably-evoked fEPSPs ($>20\%$ baseline) across the MED-64 probe with increasing stimulus intensity in naïve, saline (Sal-control), BV-inflamed and bupivacaine-blocked before BV injection (Block) groups of slices. The number of slices for each group is shown in parentheses. ****** $P < 0.01$ vs naïve or saline-control. Mean \pm SEM.

and LTD^[31,42-44,62]. Here, we provided a new experimental paradigm that combined 2D-CSD imaging with planar MEA recordings through 8×8 (64)-channels on an intra-ACC slice preparation, allowing study of the spatial and temporal plasticity of intracortical synaptic organization at the network level.

In the current study, we first mapped the spatial and temporal localization of current sinks across layers I, II–III and V–VI evoked by stimulation of the deep layers (V–VI). The deep layers of the ACC are the loci of pain-related neuronal somata, and some of the pyramidal cells have recurrent axon collaterals that spread from deep (V–VI) to superficial (II–III) layers, forming intra-ACC synaptic connections^[33,36]. Besides, some medial thalamus–ACC projection fibers enter the superficial ACC through these deep layers^[31]. Thus, the intra-ACC synaptic

organization described here was formed by both intra-cortical and extra-cortical input sources. Under naïve conditions, the current sink shown by 2D-CSD images was initially generated in layer VI followed by spread from layer VI to layer V and was finally confined to layers II–III. This spatial pattern of sink movement is likely to reflect dynamic changes in depolarization sites first at the pain-related neuronal somata in layers V–VI, then activation from layer VI to layer V, and finally to layers II–III, where intra-cortical recurrent axon collaterals and extra-cortical inputs terminate. These spatial time-varying scenarios of activation (current sinks) in the ACC reflected a spatial change of postsynaptic events mediated by glutamate ionic receptors. Based on pharmacological identification, the components of each LFP in the different layers were characterized. We found that the late components (N2 and

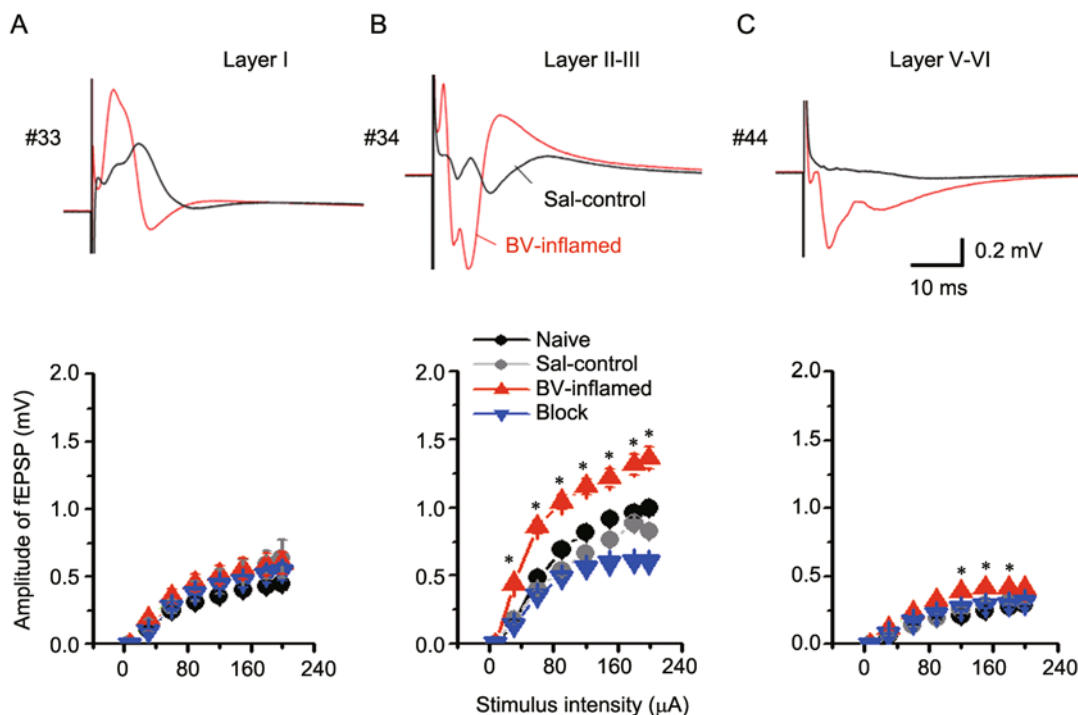


Fig. 7. Layer-specific stimulus intensity-network response curves in the ACC. Upper panels in A–C show typical LFP traces recorded in layers I, II/III and V/VI with saline or BV injection. Vertical scale indicates amplitude, horizontal scale indicates time. Lower panels in A–C show the input-output curves of layers I, II/III and V/VI for the different groups. * $P < 0.05$ vs naive or saline-control. Mean \pm SEM.

P2) in layers II–III and the late components (N1 and P2) in V–VI were fEPSPs because they were deleted or inhibited by hMg-ICa and CNQX. In contrast, the early part of P1 components in layers I, II–III and V–VI were presynaptic volleys because they were resistant to hMg-ICa and CNQX but sensitive to TTX. These events evoked in the ACC by deep-layer stimulation are mostly consistent with those described previously^[31,44]. Since the remaining early N1 component in layers II–III was resistant to TTX, hMg-ICa and CNQX, it was probably a non-synaptic event caused by the recurrent collaterals of layer V pyramidal cells as suggested in previous reports^[31,33,36,44]. The only difference between our and previous results is that we demonstrated the non-involvement of glutamate NMDA receptors in the generation of current sinks as well as LFPs evoked by stimulation of deep layers, while other reports have shown that NMDA receptors are involved in the late components of LFPs^[31,44,62]. This is probably due to the difference in electrical intensity used for pharmacological investigations: we used the half-maximal response (80–90 μ A) as the test stimulus, while in previous studies the maximal intensity

(200 μ A) was used^[44]. The weak intensity used may not have been able to activate NMDA receptors, leading to the absence of NMDA receptor-mediated components. Regarding this possibility, the effects of NMDA receptors on LFPs induced by high-intensity electrical stimulation will be examined in our future experiments. Another explanation might be that these spatial plastic changes are NMDA-independent^[64]. This has been reported in the hippocampal formation^[48], and it has been suggested that a mechanism for pain information processing that is different from learning and memory may exist in higher brain regions^[48,64].

To address whether peripheral inflammatory pain can change the stability of intra-ACC synaptic organization (network), we pre-conditioned rats with 2 h of persistent nociception by intraplantar injection of BV. After this pre-conditioning, the spatial profile of intra-ACC synaptic organization was significantly changed, showing an enlarged current sink distribution and a leftward shift of the stimulus-response curves relative to naive and saline-control rats. The spatial change was greatest in layers II–III where synaptic connections are densely localized^[65]. The

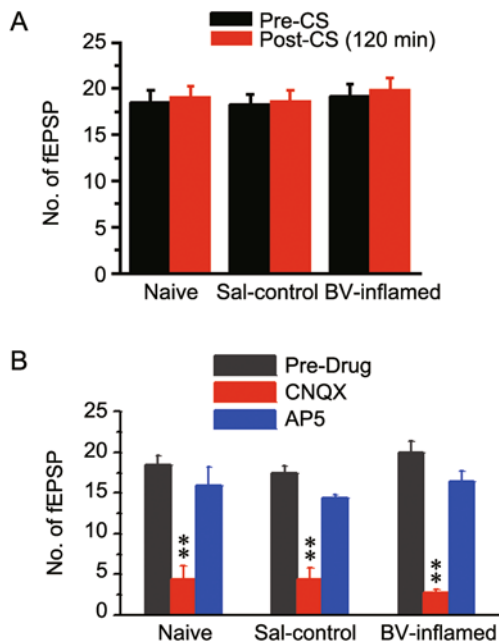


Fig. 8. Effects of LTP conditioning or drugs on intra-ACC synaptic network profiles in slices from naïve, saline-control and BV-inflamed rats. **A:** Effects of CS on the mean total number of fEPSPs recorded across MED-64 probes in the ACC from naïve, saline (Sal-control) and BV-inflamed groups. **B:** Effects of CNQX (10 $\mu\text{mol/L}$) and AP5 (100 $\mu\text{mol/L}$) on the mean total number of fEPSPs in the ACC. Pre-CS, pre-conditioning stimulus; Post-CS, post-conditioning stimulus. ** $P < 0.01$ vs pre-drug. Mean \pm SEM.

spatial expansion in the ACC observed in the current study was tightly linked to the effect of BV-induced inflammatory pain, because bupivacaine blockade at the site of BV injection completely eliminated the spatial re-organization of network synaptic connections. These results suggested that the stability of intra-ACC synaptic organization can be altered by pre-conditioning nociceptive input, probably leading to fear, anxiety-like and depression-like behaviors^[66-69]. It is worthy of note that since BV contains many bioactive substances that may cause itch and other non-painful sensations^[38], we could not completely exclude the roles of non-painful sensory inputs in the neuronal plasticity observed in the current study^[70,71].

As for the temporal properties, the LTP induction rate was tested first. In layers II–III of the ACC slice, LTP induction was significantly increased in both the saline- and BV-treated groups compared to naïve rats,

suggesting that both transient and persistent nociceptive input can change the LTP induction rate in the superficial layers (II–III). However, in the deep layers (V–VI), the LTP induction was specifically increased by BV-conditioning compared with naïve and saline-control, implying that persistent nociceptive input alone can change the LTP induction rate in the deep layers. Unlike the induction rate, BV-conditioning did not change the magnitude of LTPs recorded over 2 h. Taken together, the BV-induced inflammatory pain state can result in distinct spatial and temporal plasticity of synaptic organization in the ACC that may underlie the spatial enlargement and increased intensity of activation following painful stimuli revealed in other neuroimaging studies^[6,7,16,22].

Possible Mechanisms of Spatial Plasticity

Generally, the mechanisms underlying the enlarged neuronal network responses may operate in two ways. One is recruitment of more input onto previously activated synapses, and the other is an increase in the number of synaptic contacts onto more newly-activated neurons or an increase in postsynaptic dendritic spines on previously-activated cells, thus resulting in an enlarged effective network. In the present study, we probably recorded both types of functional change. Glutamate is the major excitatory neurotransmitter in the ACC^[72,73], acting on NMDA and non-NMDA receptors (AMPA/KA receptors) on the postsynaptic membrane. Our pharmacological experiments demonstrated that the evoked LFPs and current sinks in layers II–III and V–VI were mediated by glutamate non-NMDA receptor subtypes. It is known that, fast glutamatergic EPSPs are mediated by AMPA/KA receptors, while the action of glutamate through NMDA receptors is conducted in a voltage-dependent manner, as the ionic NMDA channel is blocked by Mg^{2+} at resting membrane potentials^[74-76]. Thus, at resting membrane potentials most glutamatergic synaptic responses are carried out by AMPA/KA receptors, while the activation of NMDA receptors may only have little contribution.

Our findings that the enhanced synaptic transmission and the enlarged spatial profile of intra-ACC synaptic organization were principally mediated by NMDA-independent mechanisms suggested the existence of a unique underlying mechanism involving neuronal circuits for modulating the synaptic organization. This presumption

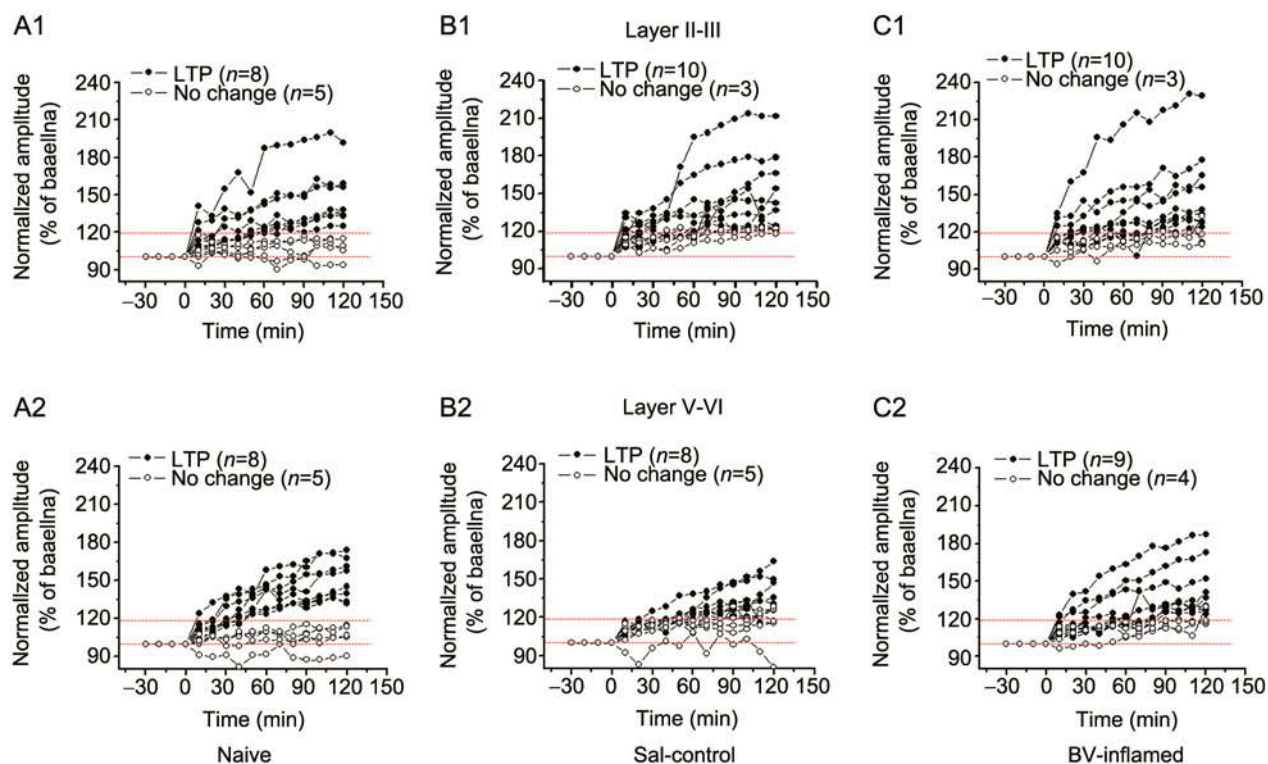


Fig. 9. Induction of LTP in layers II/III and V/VI of the ACC from naïve, saline-control and BV-inflamed rats. A1–C1: Induction rates of LTP in layers II/III under different states. A2–C2: Induction rates in layers V/VI under different states. The number of slices is indicated in parentheses.

is largely supported by our previous results. In that study, by using patch clamp recordings, both excitatory and inhibitory post-synaptic responses in the ACC were recorded under the same experimental protocol as the current study. Briefly, the excitatory synaptic transmission was enhanced while the inhibitory synaptic transmission was decreased by persistent peripheral nociception^[39]. The enhanced excitatory synaptic transmission is likely to be attributable to both the increased probability of pre-synaptic excitatory neurotransmitter (e.g., glutamate) release and the increased availability of postsynaptic receptors in the ACC^[39,76–78]. Whereas the resultant decreased inhibitory synaptic transmission is likely due to the decreased responsiveness or loss of inhibitory post-synaptic receptors (e.g., GABA) or altered intrinsic synaptic properties of inhibitory synaptic modulation in the ACC^[39,79,80]. Collectively, we propose that enlarged synaptic connections or altered intra-ACC synaptic functional organization induced by persistent peripheral nociception may be

produced by decreased or lost tonic inhibition mediated by GABAergic interneurons through mechanisms that remain to be investigated.

An imbalance of excitatory and inhibitory synaptic transmission also occurs in the hippocampal formation following persistent nociception with the same technique^[45,47], a region that is associated with cognitive impairment induced by pain, which is also one of its comorbidities^[81]. Thus, the characterization of neuronal circuits in the cortical and subcortical structures involved in pain information processing at the network level is important in the search for the mechanisms underlying the pain comorbidities, e.g. anxiety and depression.

Possible Mechanisms of Temporal Plasticity

LTP is believed to play a key role in information processing in the mammalian brain, and LTP in the ACC is associated with chronic pain, as well as pain-related cognitive emotional disorders^[19,21]. The form of LTP may vary

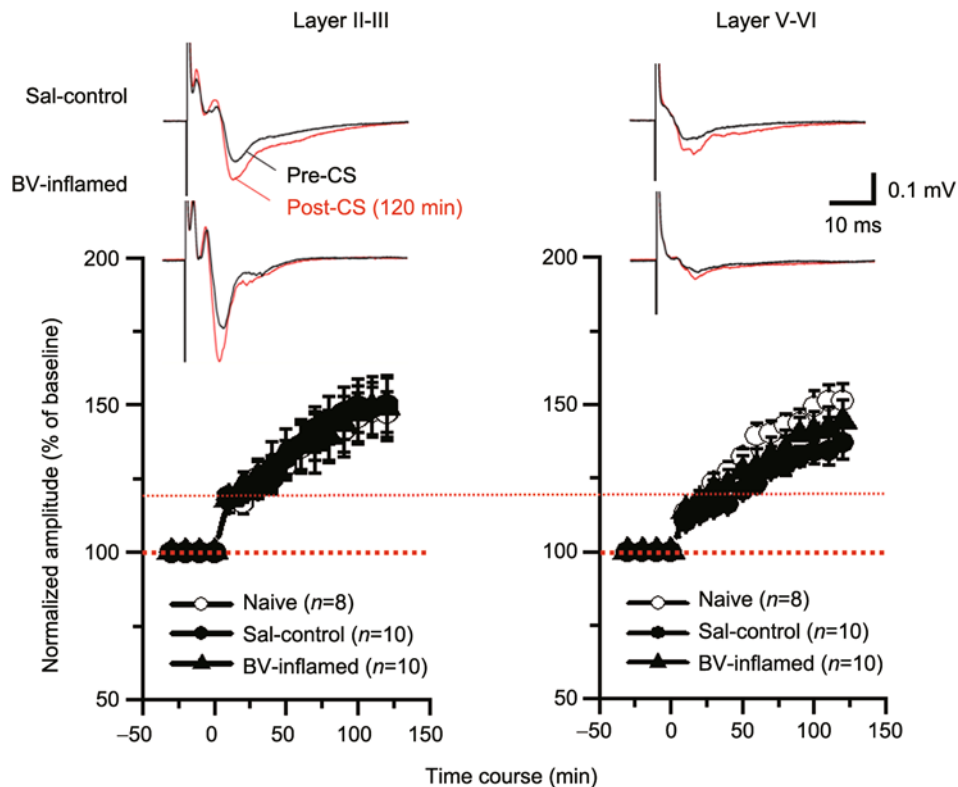


Fig. 10. Effects of inflammatory pain on LTP magnitude across layers II-III and V-VI in the ACC. Upper panels: example traces of LFPs in layers II-III (left) and V-VI (right) prior to and 120 min after pre-conditioning. Lower panels: the amplitudes of both layers II-III and V-VI fEPSPs were normalized as a percentage of the pre-conditioning baseline and plotted as a function of time. The number of slices used to plot the graph is indicated in parentheses. Vertical scale indicates amplitude, horizontal scale indicates time. Mean \pm SEM.

with different pre-conditioning stimuli or across various brain areas^[64,82]. Moreover, the mechanisms underlying its induction and maintenance may differ with different experimental protocols^[64,82]. As has been suggested by Raymond (2007)^[64], at least three forms of LTP can be induced experimentally: (1) LTP1 (also referred to as early LTP) is a rapidly-decaying and protein synthesis-independent process that may involve post-translational modification of various synaptic proteins or protein kinases; (2) LTP2 is an intermediate phase of late LTP that requires protein synthesis but is independent of gene transcription; and (3) LTP3 is equivalent to late LTP that requires both protein synthesis and gene transcription. Generally, LTP1 can only be induced by weak brief TBS (1 train) and occurs selectively in dendritic spines, involving the activation of NMDA receptors and Ca^{2+} -induced Ca^{2+} release (CICR) through ryanodine and IP_3 (inositol [1,4,5]-trisphosphate)

receptors; LTP2 can be induced by short-train TBS (4–5 trains) and selectively occurs in dendrites, requiring synchronization of both NMDA and mGluRs that lead to the involvement of protein kinase C and CICR through IP_3 and protein synthesis through ERK activation; and LTP3 can only be induced by strong long-train TBS (8–10 trains) and involves somatic signaling mechanisms that are dependent upon L-type voltage-dependent Ca^{2+} channels (VDCCs), leading to gene transcription through cAMP response-element binding protein. Based on these definitions of LTP, we suggest that the distinct form of LTP induced in the ACC neuronal network in the current study was LTP3 (NMDA-independent but probably VDCC-dependent). This inference is supported by at least three experimental conditions: (1) the pre-conditioning stimulus protocol we used was long-train TBS (10 trains) that has been suggested to be enough to induce LTP3 by Raymond

(2007)^[64] and has a high induction rate according to our previous experiments^[42]; (2) bath perfusion of hMg-ICa solution blocked the post-synaptic components of fEPSPs, but AP5, an NMDA glutamate receptor antagonist, failed to do so, suggesting the involvement of Ca²⁺ inflow through VDCCs rather than NMDA receptors; and (3) the involvement of non-NMDA receptors. Moreover, spike discharges in the pyramidal neurons of layers III–V are increased by increasing stimulus frequency under the BV-induced persistent pain state compared with the naïve and saline-control conditions, suggesting that the membrane depolarization is frequency-dependent^[39].

Unlike that in the hippocampal formation^[48], the LTP magnitude induced in the ACC was not enhanced by persistent peripheral nociception in comparison with the naïve and saline-control conditions in the current study. The reasons for this disparity remain unknown and are worthy of further study. Because the pre-conditioning protocol for LTP induction and the experimental procedures with MEA are similar in the hippocampal and ACC experiments, regional differences should also be taken into account. LTP in the ACC has been well studied in mice^[83–87]. However, enhancement of LTP has not been directly reported in either physiological or pathological pain models, although the roles of some molecular signaling pathways in the induction of LTP have been recently revealed in transgenic and gene-knockout mice^[83–87]. Moreover, the pre-conditioning protocol for LTP induction used in those studies was usually 5 trains of TBS that has an induction rate of <25% in rats^[42]. Short trains (4–5 trains of TBS) are thought to enable the induction of LTP2^[64]. Thus, the LTP evoked in the ACC by long-train TBS under naïve and saline control conditions in the current report might have been in a ceiling state that could not be further enhanced by the pre-existing peripheral persistent pain stimulation. This presumption can be explained by the leftward shift of the I-O curve for the BV-inflamed condition, a sensitized or hyperexcitable state of ACC synaptic function, in comparison with the naïve and saline-control conditions. Moreover, this leftward shift was reversed by peripheral bupivacaine blockade of persistent BV-induced firing originating from the injection site^[38,55,56,58,88].

It is noteworthy that LTP induction in layers V–VI occurred ~30 min later than in layers II–III. As noted above,

the pyramidal cell-bodies located in layer V send apical dendrites to and receive outputs from layers II–III. It can be proposed that LTP1 and LTP2 occur at dendritic spines and dendrites, while LTP3 occurs in the proximity of the soma and involves gene expression, thus needing a longer time for its expression. Collectively, it is reasonable to argue that the LTP that we induced in layers II–III may have mixed forms of LTP with an earlier expression time, while LTP in layers V–VI where the somata of pyramidal cells are located was mainly LTP3 and thus needed a longer time to be expressed. Accordingly, this time-delay may be related to different stages (post-translation modification, protein-synthesis, and gene transcription) of synaptic plasticity at the pyramidal neurons and/or neuronal circuits formed by synaptic connections between layer III and layer V pyramidal cells. The different layer-related forms of LTP that we induced in the same ACC slice using the MEA technique may be useful for the study of temporal synaptic plasticity in spatial arrangements in the brain that remain largely unknown.

CONCLUSIONS

Two-dimensional CSD imaging of intra-ACC synaptic organization was produced by recordings through planar MEA probes with 8 × 8 (64)-channels. Spatial time-variant scenarios of current sinks (depolarization) evoked in the ACC from layers V–VI to II–III were characterized as postsynaptic events mediated by glutamate ionic receptors. The functional structure of intra-ACC synaptic organization was significantly changed by pre-conditioned peripheral persistent pain, suggesting the occurrence of pain-related spatial plasticity in the ACC. Pre-blockade of nociceptive afferent input reversed the nociception-associated plasticity. At the network level, the findings of spatial enlargement of synaptic connections and increased LTP induction rates within the ACC suggest a change in neuronal circuits by persistent pain that may involve the recruitment of new extra-cortical input, and the release of tonic inhibition through disinhibition and/or the growth of new dendritic spines.

ACKNOWLEDGMENTS

This work was supported by grants from the National Basic

Research Development Program, Ministry of Science and Technology of China (2013CB835100, 2013BAI04B04), the National Natural Science Foundation of China (81070899, 81171049) and a Military Project of China (AWS12J004).

Received date: 2013-02-25; Accepted date: 2013-04-19

REFERENCES

- [1] Giamberardino NA, Jensen TS. Pain Comorbidities: Understanding and Treating the Complex Patient. Seattle: IASP Press, 2012.
- [2] Basbaum AI, Bautista DM, Scherrer G, Julius D. Cellular and molecular mechanisms of pain. *Cell* 2009, 139: 267–284.
- [3] Fields HL. State-dependent opioid control of pain. *Nat Rev Neurosci* 2004, 5: 565–575.
- [4] Millan MJ. Descending control of pain. *Prog Neurobiol* 2002, 66: 355–474.
- [5] Porreca F, Ossipov M, Gebhart G. Chronic pain and medullary descending facilitation. *Trends Neurosci* 2002, 25: 319–325.
- [6] Apkarian AV, Bushnell MC, Treede RD, Zubieta JK. Human brain mechanisms of pain perception and regulation in health and disease. *Eur J Pain* 2005, 9: 463–484.
- [7] Apkarian AV, Hashmi JA, Baliki MN. Pain and the brain: specificity and plasticity of the brain in clinical chronic pain. *Pain* 2011, 152: S49–64.
- [8] Chang C, Shyu BC. A fMRI study of brain activations during non-noxious and noxious electrical stimulation of the sciatic nerve of the rats. *Brain Res* 2001, 897: 71–81.
- [9] Shih YY, Chen YY, Chen CC, Chen JC, Chang C, Jaw FS. Whole-brain functional magnetic resonance imaging mapping of acute nociceptive responses induced by formalin in rats using atlas registration-based event-related analysis. *J Neurosci Res* 2008, 86: 1801–1811.
- [10] Shih YY, Chiang YC, Chen JC, Huang CH, Chen YY, Liu RS, *et al.* Brain nociceptive imaging in rats using (18) f-fluorodeoxyglucose small-animal positron emission tomography. *Neuroscience* 2008, 155: 1221–1226.
- [11] Chai SC, Kung JC, Shyu BC. Roles of the anterior cingulate cortex and medial thalamus in short-term and long-term aversive information processing. *Mol Pain* 2010, 6:42.
- [12] Gao YJ, Ren WH, Zhang YQ, Zhao ZQ. Contributions of anterior cingulate cortex and amygdala to pain- and fear-conditioned place avoidance in rats. *Pain* 2004, 110: 343–353.
- [13] Johansen JP, Fields HL, Manning BH. The affective component of pain in rodents: directive evidence for a contribution of the anterior cingulate cortex. *Proc Natl Acad Sci U S A* 2001, 98: 8077–8082.
- [14] Lei LG, Sun S, Gao YJ, Zhao ZQ, Zhang YQ. NMDA receptors in the anterior cingulate cortex mediate pain-related aversion. *Exp Neurol* 2004, 189: 413–421.
- [15] Price DD. Psychological and neural mechanisms of the affective dimension of pain. *Science* 2000, 288: 1769–1772.
- [16] Rainville P, Duncan GH, Price DD, Carrier B, Bushnell MC. Pain affect encoded in human anterior cingulate but not somatosensory cortex. *Science* 1997, 277: 968–971.
- [17] Thomas GJ, Slotnick BM. Impairment of avoidance responding by lesions in cingulate cortex in rats depends on food drive. *J Comp Physiol Psychol* 1963, 56: 959–964.
- [18] Vogt BA. Pain and emotion interactions in subregions of the cingulate gyrus. *Nat Rev Neurosci* 2005, 6: 533–544.
- [19] Zhuo M. Neuronal mechanism for neuropathic pain. *Mol Pain* 2007, 3: 14.
- [20] Zhuo M. A synaptic model for pain: long-term potentiation in the anterior cingulate cortex. *Mol Cells* 2007, 23: 259–271.
- [21] Zhuo M. Cortical excitation and chronic pain. *Trends Neurosci* 2008, 31: 199–207.
- [22] Rainville P. Brain mechanisms of pain affect and pain modulation. *Curr Opin Neurobiol* 2002, 12: 195–204.
- [23] Donahue RR, LaGraize SC, Funchs PN. Electrical lesion of the anterior cingulate cortex decreases inflammatory, but not neuropathic nociceptive behavior in rats. *Brain Res* 2001, 897: 131–138.
- [24] LaGraize SC, Labuda CJ, Rutledge MA, Jackson RL, Fuchs PN. Differential effect of anterior cingulate cortex lesion on mechanical hypersensitivity and escape/avoidance behavior in an animal model of neuropathic pain. *Exp Neurol* 2004, 188: 139–148.
- [25] Pastoriza LN, Morrow TJ, Casey KL. Medial frontal cortex lesions selectively attenuate the hot plate response: possible nocifensive apraxia in the rat. *Pain* 1996, 64: 11–17.
- [26] Ren LY, Lu ZM, Liu MG, Yu YQ, Li Z, Shang GW, *et al.* Distinct roles of the anterior cingulate cortex in spinal and supraspinal bee venom-induced pain behaviors. *Neuroscience* 2008, 153: 268–278.
- [27] Vaccarino AL, Melzack R. Analgesia produced by injection of lidocaine into the anterior cingulum bundle of the rat. *Pain* 1989, 39: 213–219.
- [28] Calejesan AA, Kim SJ, Zhuo M. Descending facilitatory modulation of a behavioral nociceptive response by stimulation in the adult rat anterior cingulate cortex. *Eur J Pain* 2000, 4: 83–96.
- [29] Koyama T, Tanaka YZ, Mikami A. Nociceptive neurons in the macaque anterior cingulate activate during anticipation of pain. *Neuroreport* 1998, 9: 2663–2667.
- [30] Kung JC, Su NM, Fan RJ, Chai SC, Shyu BC. Contribution of the anterior cingulate cortex to laser-pain conditioning in rats. *Brain Res* 2003, 970: 58–72.

- [31] Lee CM, Chang WC, Chang KB, Shyu BC. Synaptic organization and input-specific short term plasticity in anterior cingulate cortical neurons with intact thalamic inputs. *Eur J Neurosci* 2007, 25: 2847–2861.
- [32] Shyu BC, Chen WF, Shih HC. Electrically and mechanically evoked nociceptive neuronal responses in the rat anterior cingulate cortex. *Acta Neurochir Suppl* 2008, 101: 23–25.
- [33] Shyu BC, Sikes RW, Vogt LJ, Vogt BA. Nociceptive processing by anterior cingulate pyramidal neurons. *J Neurophysiol* 2010, 103: 3287–3301.
- [34] Sikes RW, Vogt BA. Nociceptive neurons in area 24 of rabbit cingulate cortex. *J Neurophysiol* 1992, 68: 1720–1732.
- [35] Wu JJ, Shih HC, Yen CT, Shyu BC. Network dynamics in nociceptive pathway assessed by the neuronal avalanche model. *Mol Pain* 2012, 8: 33.
- [36] Yamamura H, Iwata K, Tsuboi Y, Toda K, Kitajima K, Shimizu N, *et al.* Morphological and electrophysiological properties of ACCx nociceptive neurons in rats. *Brain Res* 1996, 735: 83–92.
- [37] Hutchison WD, Davis KD, Lozano AM, Tasker RR, Dostrovsky JO. Pain-related neurons in the human cingulate cortex. *Nat Neurosci* 1999, 2: 403–405.
- [38] Chen J, Lariviere R. The nociceptive and anti-nociceptive effects of bee venom injection and therapy: a double-edged sword. *Prog Neurobiol* 2010, 92: 151–183.
- [39] Gong KR, Cao FL, He Y, Gao CY, Wang DD, Li H, *et al.* Enhanced excitatory and reduced inhibitory synaptic transmission contribute to persistent pain-induced neuronal hyper-responsiveness in anterior cingulate cortex. *Neuroscience* 2010, 171: 1314–1325.
- [40] Palomero-Gallagher N, Mohlberg H, Zilles K, Vogt BA. Cytology and receptor architecture of human anterior cingulate cortex. *J Comp Neurol* 2009, 508: 906–926.
- [41] Yang JW, Shih HC, Shyu BC. Introcortical circuits in rat anterior cingulate cortex are activated by nociceptive inputs mediated by medial thalamus. *J Neurophysiol* 2006, 96: 3409–3422.
- [42] He Y, Liu MG, Gong KR, Chen J. Differential effects of long and short train theta burst stimulation on LTP induction in rat anterior cingulate cortex slices: multi-electrode array recordings. *Neurosci Bull* 2009, 25: 309–318.
- [43] Kang SJ, Liu MG, Chen T, Ko HG, Baek GC, Lee HR, *et al.* Plasticity of metabotropic glutamate receptor-dependent long-term depression in the anterior cingulate cortex after amputation. *J Neurosci* 2012, 32: 11318–11329.
- [44] Lee CM, Sylantyev S, Shyu BC. Short-term synaptic plasticity in layer II/III of the rat anterior cingulate cortex. *Brain Res Bull* 2007, 71: 416–427.
- [45] Liu MG, Wang RR, Chen XF, Zhang FK, Cui XY, Chen J. Differential roles of ERK, JNK and p38 MAPK in pain-related spatial and temporal enhancement of synaptic responses in the hippocampal formation of rats: multi-electrode array recordings. *Brain Res* 2011, 1382: 57–69.
- [46] Liu MG, Lu D, Wang Y, Chen XF, Li Z, Xu Y, *et al.* Counteracting roles of metabotropic glutamate receptor subtypes 1 and 5 in regulation of pain-related spatial and temporal synaptic plasticity in rat entorhinal-hippocampal pathways. *Neurosci Lett* 2012, 507: 38–42.
- [47] Xu Y, Jin JH, Wang Y, Wang RR, Li Z, Chen J. Facilitation of synaptic transmission and connections of entorhinal-hippocampal pathway by 5-HT_{2C} receptor subtype: multi-electrode array recordings. *Acta Physiol Sin* 2012, 64: 259–268.
- [48] Zhao XY, Liu MG, Yuan DL, Wang Y, He Y, Wang DD, *et al.* Nociception-induced spatial and temporal plasticity of synaptic connection and function in the hippocampal formation of rats: a multi-electrode recording. *Mol Pain* 2009, 5: 55.
- [49] Liu MG, Chen XF, He T, Li Z, Chen J. Use of multi-electrode array recordings in study of network synaptic plasticity in both time and space. *Neurosci Bull* 2012, 28: 409–422.
- [50] Wang DD, Li Z, Chang Y, Wang RR, Chen XF, Zhao ZY, *et al.* Neural circuits and temporal plasticity in hindlimb representation of rat primary somatosensory cortex: revisited by multi-electrode array on brain slices. *Neurosci Bull* 2010, 26: 175–187.
- [51] Zimmermann M. Ethical guidelines for investigation of experimental pain in conscious animals. *Pain* 1983, 16: 109–110.
- [52] Chen J, Luo C, Li HL, Chen HS. Primary hyperalgesia to mechanical and heat stimuli following subcutaneous bee venom injection into the plantar surface of hindpaw in conscious rat: a comparative study with the formalin test. *Pain* 1999, 83: 67–76.
- [53] Lariviere WR, Melzack R. The bee venom test: a new tonic pain test. *Pain* 1996, 66: 271–277.
- [54] Li KC, Chen J. Altered pain-related behaviors and spinal neuronal responses produced by s.c. injection of melittin in rats. *Neuroscience* 2004, 126: 753–762.
- [55] Chen J, Luo C, Li HL. The contribution of spinal neuronal changes to development of prolonged, tonic nociceptive responses of the cat induced by subcutaneous bee venom injection. *Eur J Pain* 1998, 2: 359–376.
- [56] Chen J, Li HL, Luo C, Li Z, Zheng JH. Involvement of peripheral NMDA and non-NMDA receptors in development of persistent firing of spinal wide-dynamic-range neurons induced by subcutaneous bee venom injection in the cat. *Brain Res* 1999, 844: 98–105.
- [57] Chen J, Chen HS. Pivotal role of capsaicin-sensitive primary afferents in development of both heat and mechanical

- hyperalgesia induced by intraplantar bee venom injection. *Pain* 2001, 91: 367–376.
- [58] Du YR, Xiao Y, Lu ZM, Ding J, Xie F, Fu H, *et al.* Melittin activates TRPV1 receptors in primary nociceptive sensory neurons via the phospholipase A2 cascade pathways. *Biochem Biophys Res Commun* 2011, 408: 32–37.
- [59] Wang CM, Yang L, Lu D, Lu YF, Chen XF, Yu YQ, *et al.* Simultaneous multisite recordings of neural ensemble responses in the motor cortex of behaving rats to peripheral noxious heat and chemical stimuli. *Behav Brain Res* 2011, 223: 192–202.
- [60] Chen HS, Chen J, Chen J, Guo WG, Zheng MH. Establishment of bee venom-induced contralateral heat hyperalgesia in the rat is dependent upon central temporal summation of afferent input from the site of injury. *Neurosci Lett* 2001, 298: 57–60.
- [61] Paxinos G, Watson C. The rat brain in stereotaxic coordinates. 5th ed. Amsterdam: Elsevier Academic Press, 2005: 367.
- [62] Chang WC, Lee CM, Shyu BC. Temporal and spatial dynamics of thalamus-evoked activity in the anterior cingulate cortex. *Neuroscience* 2012, 222: 302–315.
- [63] Shyu BC, Vogt BA. Short-term synaptic plasticity in the nociceptive thalamic-anterior cingulate pathway. *Mol Pain* 2009, 5: 51.
- [64] Raymond CR. LTP forms 1, 2 and 3: different mechanisms for the “long” in long-term potentiation. *Trends Neurosci* 2007, 30: 167–175.
- [65] Wang CC, Shyu BC. Differential projections from the mediodorsal and centrolateral thalamic nuclei to the frontal cortex in rats. *Brain Res* 2004, 995: 226–235.
- [66] Narita M, Kuzumaki N, Narita M, Kaneko C, Hareyama N, Miyatake M, *et al.* Chronic pain-induced emotional dysfunction is associated with astrogliosis due to cortical delta-opioid receptor dysfunction. *J Neurochem* 2006, 97: 1369–1378.
- [67] Schellinck HM, Stanford L, Darrah M. Repetitive acute pain in infancy increases anxiety but does not alter spatial learning ability in juvenile mice. *Behav Brain Res* 2003, 142: 157–165.
- [68] Suzuki T, Amata M, Sakaue G, Nishimura S, Inoue T, Shitaba M, *et al.* Experimental neuropathy in mice is associated with delayed behavioral changes related to anxiety and depression. *Anesth Analg* 2007, 104: 1570–1577.
- [69] Wang J, Goffer Y, Xu D, Tukey DS, Shamir DB, Eberle SE, *et al.* A single subanesthetic dose of ketamine relieves depression-like behaviors induced by neuropathic pain in rats. *Anesthesiology* 2011, 115: 812–821.
- [70] Mochizuki H, Tashiro M, Kano M, Sakurada Y, Itoh M, Yanai K. Imaging of central itch modulation in the human brain using positron emission tomography. *Pain* 2003, 105: 339–346.
- [71] Mochizuki H, Sadato N, Saito DN, Toyoda H, Tashiro M, Okamura N, *et al.* Neural correlates of perceptual difference between itching and pain: a human fMRI study. *Neuroimage* 2007, 36: 706–717.
- [72] Wei F, Li P, Zhuo M. Loss of synaptic depression in mammalian anterior cingulate cortex after amputation. *J Neurosci* 1999, 25: 11107–11116.
- [73] Wu LJ, Zhao MG, Toyoda H, Ko SW, Zhuo M. Kainate receptor-mediated synaptic transmission in the adult anterior cingulate cortex. *J Neurophysiol* 2005, 94: 1805–1813.
- [74] Nicoll RA, Kauer JA, Malenka RC. The current excitement in long-term potentiation. *Neuron* 1988, 1: 97–103.
- [75] Sah P, Nicoll RA. Mechanisms underlying potentiation of synaptic transmission in rat anterior cingulate cortex *in vitro*. *J Physiol* 1991, 433: 615–630.
- [76] Wu LJ, Toyoda H, Zhao MG, Lee YS, Tang J, Ko SW, *et al.* Upregulation of forebrain NMDA NR2B receptors contributes to behavioral sensitization after inflammation. *J Neurosci* 2005, 25: 11107–11116.
- [77] Xu H, Wu LJ, Wang H, Zhang X, Vadakkan KI, Kim SS, *et al.* Presynaptic and postsynaptic amplifications of neuropathic pain in the anterior cingulate cortex. *J Neurosci* 2008, 28: 7445–7453.
- [78] Zhao MG, Ko SW, Wu LJ, Toyoda H, Xu H, Quan J, *et al.* Enhanced presynaptic neurotransmitter release in the anterior cingulate cortex of mice with chronic pain. *J Neurosci* 2006, 26: 8923–8930.
- [79] Wang H, Ren WH, Zhang YQ, Zhao ZQ. GABAergic disinhibition facilitates polysynaptic excitatory transmission in rat anterior cingulate cortex. *Biochem Biophys Res Commun* 2005, 338: 1634–1639.
- [80] LaGraize SC, Fuchs PN. GABAA but not GABAB receptors in the rostral anterior cingulate cortex selectively modulate pain-induced escape/avoidance behavior. *Exp Neurol* 2007, 204: 182–194.
- [81] Moriarty O, McGuire BE, Finn DP. The effects of pain on cognitive function: a review of clinical and preclinical research. *Prog Neurobiol* 2011, 93: 385–404.
- [82] Byrne JH, Labar KS, Ledoux JE, Schafe GE, Sweatt JD, Thompson RF. Learning and memory: basic mechanisms. In: *From Molecules to Networks: An introduction to Cellular and Molecular Neuroscience* (Byrne JH, Roberts JL, eds). Amsterdam: Academic Press, 2009: 539–608.
- [83] Li XY, Ko HG, Chen T, Descalzi G, Koga K, Wang H, *et al.* Alleviating neuropathic pain hypersensitivity by inhibiting PKMzeta in the anterior cingulate cortex. *Science* 2010, 330: 1400–1404.
- [84] Liauw J, Wu LJ, Zhuo M. Calcium-stimulated adenylyl cyclases required for long-term potentiation in the anterior cingulate cortex. *J Neurophysiol* 2005, 94: 878–882.

- [85] Toyoda H, Zhao MG, Ulzhofer B, Wu LJ, Xu H, Seeburg PH, *et al.* Roles of AMPA receptor subunit GluA1 but not GluA2 in synaptic potentiation and activation of ERK in the anterior cingulate cortex. *Mol Pain* 2009, 5: 46.
- [86] Wei F, Qiu CS, Kim SJ, Muglia L, Maas JW, Pineda VV, *et al.* Genetic elimination of behavioral sensitization in mice lacking calmodulin-stimulated adenylyl cyclases. *Neuron* 2002, 36: 713–726.
- [87] Zhao MG, Toyoda H, Lee YS, Wu LJ, Ko SW, Zhang XH, *et al.* Roles of NMDA NR2B subtype receptor in prefrontal long-term potentiation and contextual fear memory. *Neuron* 2005, 47: 859–872.
- [88] You HJ, Chen J, Morch CD, Arendt-Nielsen L. Differential effect of peripheral glutamate (NMDA, non-NMDA) receptor antagonists on bee venom-induced spontaneous nociception and sensitization. *Brain Res Bull* 2002, 58: 561–567.